Efficient Numerical Modeling of Random Rough Surface Effects for Interconnect Internal Impedance Extraction

Quan Chen and Ngai Wong
Department of Electrical and Electronic Engineering
The University of Hong Kong,
Hong Kong
E-mail: {quanchen, nwong}@eee.hku.hk

Abstract— This paper proposes an efficient model for numerically evaluating the impact of random surface roughness on the internal impedance for large-scale interconnect structures. The effective resistivity (ER) and effective permeability (EP) are numerically formulated to avoid the computationally prohibitive global discretization, while maintaining the model accuracy and flexibility. A modified stochastic integral equation (SIE) method is proposed to significantly speed up the computation for the mean values of ER and EP under the assumption of random surface roughness. Numerical experiments then verify the efficacy of our approach.

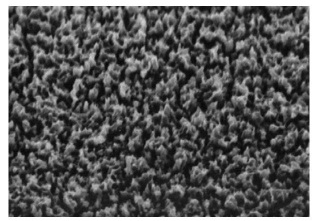

(a) Surface after etching process

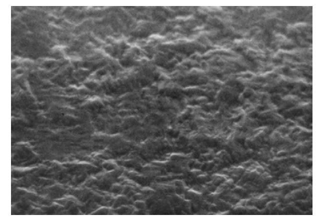

(b) Surface after annealing process

Fig. 1. SEM images of conductor surface topologies with different treatments.

I. Introduction

Owing to the ever-increasing operating frequencies and steadily decreasing feature sizes, interconnect structures of integrated circuits (IC) nowadays are modeled as a network of multiconductor transmission lines (MTLs) [1]. The effects of imperfect conductors in the MTLs model are generally represented by the frequency-dependent internal impedance $Z = R + j\omega L$ where R denotes the ohmic resistance and L denotes the internal inductance. A large body of work has been documented for the extraction of this parameter. All of them, however, only work with the pre-assumption that the conductor surfaces are perfectly smooth, at least along the direction of conducting current. Experiments have shown that many fabrication processes in IC manufacture like electronic deposition, chemical etching and annealing processes will inevitably produce conductors with surface variations. The surface roughness influences the internal impedance via prolonging the path that current travels along, which subsequently increases the resistance as well as the internal inductance. This impact is insignificant at lower frequencies where, due to the large skin depth, only a small portion of current is influenced, but is becoming remarkable as the frequency advances into the multi-GHz domain where the skin depth is comparable to the dimension of surface roughness. For example it has been reported in experiments [2] that surface roughness can increase the high-frequency resistance by a factor up to 3. Fig. 1 shows the SEM (Scanning Electron Microscope) images for the rough surface topologies in PCB interconnects under different treatment [3].

Directly incorporating the consideration of surface roughness into large-scale interconnect extraction is computationally prohibitive due to the need of modeling the complicated electromagnetic (EM) effects and the very fine discretization required to capture the rough surface details. The impact of surface roughness on resistance in modern IC design and simulation thus is commonly handled by the analytical formula [4]

$$\sigma_e = \sigma \left[1 + \frac{2}{\pi} \tan^{-1} \left(1.4 \frac{h}{\delta} \right)^2 \right]^{-1}, \tag{1}$$

where σ_e is the effective conductivity (EC), h is the RMS height of the roughness and δ is the skin depth. However, since only h is incorporated in the formula, (1) fails to differentiate different patterns and settings of roughness as long as they share the same RMS height, rending it inaccurate and inflexible for most cases. A viable compromise is to fully model the rough surface effects within a local scope and then extrapolate the results to the entire problem domain, justified by that the roughness characteristics should be globally homogeneous under given technical specifications. Proekt and Cangellaris have first analytically formulated the EC for periodical rough surface by equating the ohmic power loss in a rough surface conductor and its counterpart with smooth surface [5], whose derivation, however, is only valid when the roughness is far smaller than the skin depth. Chen and Wong have later developed a numerical formulation for the EC that is generally applicable which is solved by the stochastic integral equation (SIE) method [6], but the computation

978-1-4244-1922-7/08/$25.00 ©2008 IEEE

is expensive due to a second-order scheme introduced to remedy the error resulted from the crucial uncorrelatedness assumption.

In this paper, we introduce a concept of effective permeability (EP) μ_e, which is analogous to the EC, to model the rough surface effect on internal inductance via the magnetic energy equivalence. The combination of the EP and the effective resistivity (ER) ρ_e, the inverse of EC, enables a complete modeling of the impact of surface roughness on the internal impedance for large-scale interconnect extraction under the quasi-magnetostatic assumption. We also develop a improved formulation for the SIE method in [6] to address the computational bottleneck in the second-order correction scheme via halving the dimension of infinite integral required in the matrix elements generation. Numerical experiments are conducted to verify the efficacy of the proposed approach.

II. Problem Geometry

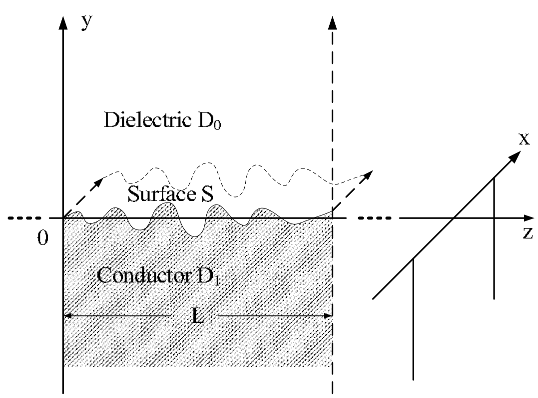

Fig. 2. Problem geometry.

As shown in Fig. 2, we consider a sampling section extracted from a long conductor, with length l and a rectangular cross section. We assume that only 1D Gaussian roughness exists along the top surface in the $z-y$ plane, while it is uniform in the x-direction. Although it is more precise to treat the realistic roughness as two-dimensional, a 1D surface model could provide a sufficient evaluation of the rough surface effects as the longitudinal roughness has the dominant influence on the internal impedance. Therefore, the problem is confined in the $z-y$ plane, composing of a dielectric region denoted as D_0 with permeability μ_0 and permittivity ϵ_0, and a conducting region denoted as D_1 with permeability $\mu=\mu_0$ and resistivity ρ. S denotes the interface between the two regions. The time-harmonically varying magnetic field $H_x(z,y)$ under study has only x component and is a function of both y and z.

III. Derivation of Effective Resistivity & Effective Permeability

For mathematical coherence, we use the effective resistivity (ER) as the metric of rough surface effects in the resistance extraction, which is simply the inverse of EC. As derived in [6], the ohmic power loss within a rough surface conductor with length l and a unit width is given by

$$P_r = \frac{\rho H_0^*}{2}\,\mathrm{Re}\left\{\int_l \mathrm{d}z U(z)\right\}, \tag{2}$$

where $*$ denotes the complex conjugate and $\mathrm{Re}\{\circ\}$ denotes the real part. H_0 is an arbitrary constant resulting from the application of Dirichlet boundary condition [7] and

$$U(z) = \sqrt{1+\left(\frac{dy(z)}{dz}\right)^2}\left(\frac{\partial H_x(z,y(z))}{\partial n}\right)_{z\in\, l} \tag{3}$$

corresponds to the normal derivative of the magnetic field on the rough surface. It should be noted that the validity of the Dirichlet boundary condition is justified by the fact that the typical dimension of surface roughness is small when compared to the overall problem dimensions [7], i.e., the thickness for top/bottom roughness, the width for sidewall roughness and the separation among conductors.

If the surfaces are plane, the power dissipated in the same conductor would be

$$P_s = \frac{\rho\left|H_0\right|^2 l}{2\delta}, \tag{4}$$

where the skin depth $\delta=\sqrt{1/(2\pi f\mu\sigma)}$ with f being the frequency. In view of the energy equivalence $P_r=P_s$, the ER ρ_e is defined as

$$\rho_e = \frac{2P_r\delta}{\left|H_0\right|^2 l} \tag{5}$$

such that $P_r=\rho_e\left|H_0\right|^2 l/(2\delta)$.

Similarly, the formulation of the EP begins with the computation of the magnetic energy stored in the rough surface conductor

$$\begin{aligned}
W_r &= \mu\int_V H_x H_x^*\mathrm{d}v \\
&= \frac{\mu}{2}\int_V (H_x^* H_x + H_x H_x^*)\mathrm{d}v \\
&= \frac{\mu\delta^2}{4j}\int_V (H_x^*\nabla^2 H_x - H_x\nabla^2 H_x^*)\mathrm{d}v \\
&= \frac{\mu\delta^2}{4j}\int_S (H_x^*\frac{\partial H_x}{\partial n} - H_x\frac{\partial H_x^*}{\partial n})\mathrm{d}s \\
&= \frac{\mu\delta^2 H_0^*}{2}\mathrm{Im}\left\{\int_S \frac{\partial H_x}{\partial n}\mathrm{d}s\right\} \\
&= \frac{\mu\delta^2 H_0^*}{2}\mathrm{Im}\left\{\int_l U(z)\mathrm{d}z\right\},
\end{aligned} \tag{6}$$

where $\mathrm{Im}\{\circ\}$ denotes the imaginary part. The third equality results from the Helmholtz equation $\nabla^2 H_x = (2j/\delta^2)H_x$. The fourth equality applies the Green's second identity and the similar approximation in the Apendix I in [7]. The last equality is due to the projection of integral domain.

The magnetic energy stored in the smooth surface counterpart is

$$W_s = \frac{\mu\delta \left|H_0\right|^2 l}{2}. \tag{7}$$

Following the energy equivalence $W_r = W_s$, we derive the EP μ_e as

$$\mu_e = \frac{2W_r}{\delta \left|H_0\right|^2 l}. \tag{8}$$

Hence, the whole problem boils down to the computation of $U(z)$, which can be readily solved from the following governing equation [6]

$$\int_l \mathrm{d}z \sum_{q=-Q}^{Q} G(z+ql, y; z', y')U(z) = \frac{1}{2}H_0 + H_0 \int_{l(z\neq z')} \mathrm{d}z \sum_{q=-Q}^{Q} \frac{\partial G(z+ql, y; z', y')}{\partial n}, \tag{9}$$

where G refers to the Green's function and $Q = 20\delta/L$.

Since the surface roughness in reality is essentially random, we need a statistical solver to compute the statistical average for the ER and EP. Once the statistical ER and EP are computed, they can be readily applied to various existing extraction engines like FastHenry [8] to appropriately evaluate the impact of surface roughness without modifying the kernel formulae. The commonly used tool for statistical computation is the Monte-Carlo (MC) simulation [9], which, however, frequently suffers from its slow convergence [10]. A non-MC alternative, SIE method, is firstly proposed in [11], [12] for rough surface capacitance extraction. It is later extended in [6] for the resistance case. In the following section, we first give a brief summary of the original SIE method and then propose a new formulation of the SIE method to significantly enhance its efficiency.

IV. Efficient Formulation of SIE Method

A. Original SIE method

The fundamental idea of the SIE method is to establish a statistical format (10) for the governing equation (9) so that the statistical solution $< U(z) >$ ($< \circ >$ denotes the ensemble average) could be obtained in one run [6], in contrast to the thousands of runs required in the MC simulation.

$$\int_l \mathrm{d}z \sum_{q=-Q}^{Q} < G(z+ql, y; z', y') >< U(z) >= \frac{1}{2}H_0 + H_0 \int_{l(z\neq z')} \mathrm{d}z \sum_{q=-Q}^{Q} < \frac{\partial G(z+ql, y; z', y')}{\partial n} > \tag{10}$$

The complete flow of computing the statistical ER by the SIE method is summarized as blow (hereafter we use $\bar{X}$ to stand for the mean value of a variable X):

$$\bar{\rho}_e = \delta \bar{P}_r/(2l), \tag{11}$$

$$\bar{P}_r = \bar{P}_r^{(0)} + \bar{P}_r^{(2)}, \tag{12}$$

$$\bar{P}_r^{(0)} = \rho \mathrm{Re}\left\{\bar{V}^T \bar{U}^{(0)}\right\}, \tag{13}$$

$$\bar{P}_r^{\ (2)} = \rho \mathrm{Re}\left\{\mathrm{trace}(\bar{A}^{-T} D)\right\}, \tag{14}$$

$$\bar{U}^{(0)} = \bar{A}^{-1}\bar{V}, \tag{15}$$

$$\mathrm{vec}(D) = F(\bar{U}^{(0)} \otimes \bar{U}^{(0)}), \tag{16}$$

where H_0 is set to be 2 and the definition of the operators *vec* and $\otimes$ can be referred to [10]. The mean value of the EP could be obtained from above formula by replacing ρ with μ, P_r with W_r, and Re with Im. It should be noted the the second integral term on the right hand side of (10) vanishes due to the opposite monotonity of probability density function and the normal derivative of the Green's function, and thus the whole right hand side of (10) could be readily represented by a constant column vector $\bar{V}_i = \Delta z$ with Δz being the panel size. The entries of $\bar{A}$ and F are formulated as follows:

$$\bar{A}_{ik} = \sum_{q=-Q}^{Q} \int \mathrm{d}y_i \int \mathrm{d}y_k P_2(y_i, y_k; z_i+ql, z_k) \cdot \int_{\Delta z_i} \mathrm{d}z_i \int_{\Delta z_k} \mathrm{d}z_k G(z_i+ql, y_i; z_k, y_k) \tag{17}$$

$$F_{mn}^{ik} =< A_{ik}A_{mn} > - \bar{A}_{ik}\bar{A}_{mn}, \tag{18}$$

$$< A_{ik}A_{mn} >= \int \mathrm{d}y_i \int \mathrm{d}y_k \int \mathrm{d}y_m \int \mathrm{d}y_n \, P_4(y_i, y_k, y_m, y_n; z_i, z_k, z_m, z_n) A_{ik}A_{mn}, \tag{19}$$

where z_i is the centroid of the ith panel and P_{N_p} stands for the N_p dimensional joint Gaussian distribution function

$$P_{N_p}(Y, Z) = \frac{1}{(2\pi)^{N_p/2} h^{N_p} \left|\Sigma\right|^{1/2}} \exp\left(-\frac{Y\Sigma^{-1}Y^T}{2h^2}\right), \tag{20}$$

where h is the RMS height and $Y = [y_1, ..., y_{N_p}], Z = [z_1, ..., z_{N_p}]$. The Σ is the correlation matrix with $\Sigma_{ij} = \exp(-(z_i - z_j)^2/\eta^2)$, $\quad i, j = 1, 2, ..., N_p$, where η is the correlation length.

B. Improved formulation of SIE method

Though with many fascinating features, the original version of the SIE method in [6] does not exhibit adequate superiority in efficiency when compared to the MC-based method, which could be attributed to the relatively slow second-order correction scheme, (14) and (16), developed for remedying the error due to the crucial uncorrelatedness assumption [11]. A major computational bottleneck lies in the involvement of high dimensional infinite integral. As shown in (19), the generation of each entry in F involves a 4D infinite integral. The standard numerical technique for computing infinite integral is the Gauss Hermite quadrature [13], which has a poor performance for higher dimensional cases due to the "curse of dimensionality", i.e., the complexity grows exponentially with the integral dimension. The situation becomes especially worse for the strongly correlated region where a large number

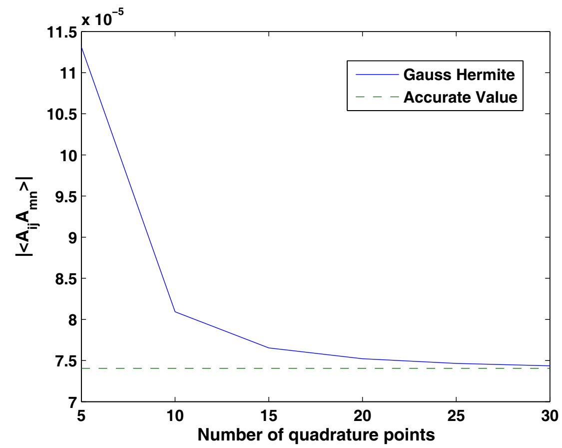

Fig. 3. Gauss Hermite quadrature.

of quadrature points are required to capture the rapid change of function value. Fig.3 depicts the value of $| < A_{ik}A_{mn} > |$ with $[i, k, m, n] = [1, 2, 3, 4]$ calculated by the Gauss Hermite quadrature with respect to the number of quadrature points used in each dimension of infinite integral. The panel size is $\Delta z = \eta/4$. It is seen that more than 20 points are required to maintain a satisfactory accuracy, which leads to an overall $O(20^4)$ complexity for the computation of just one entry in F.

MC integration is usually the only alternative for high dimensional integral owing to its dimension-independent complexity. Nevertheless, the MC integration also produces probabilistic results, say, the mean and variance we calculated are also random, and the number of runs needed to make the results converge to relatively stable ones is often very large. In the following, we demonstrate a new formulation for the SIE method in which the dimension of infinite integral is halved thereby the Gauss Hermite quadrature remains feasible to produce deterministic results. For simplicity, we first discuss a 2D case

$$\bar{A}_{ik} = \int \mathrm{d}y_i \int \mathrm{d}y_k P_2(y_i, y_k; z_i, z_k) G(y_i, z_i; y_k, z_k). \quad (21)$$

One important property of the Green's function is the translation invariance

$$G(y_i, z_i; y_k, z_k) = G(y_i - y_k, z_i; 0, z_k) = \hat{G}(y_d; z_i, z_k). \quad (22)$$

where $y_d = y_i - y_k$. Equation (22) implies that it is actually unnecessary to know the probability of every combination of $[y_i, y_k]$ and what really counts is the probability of their difference y_d. All cases of $[y_i, y_k]$ that have the same difference can be merged as one case such that the computation is significantly relieved. Let $\hat{P}_1$ be the probability distribution function of y_d, (21) can be simplified as

$$\bar{A}_{ik} = \int \mathrm{d}y_d \hat{P}_1(y_d; z_i, z_k) \hat{G}(y_d; z_i, z_k). \quad (23)$$

in which the infinite integral dimension is halved. $\hat{P}_1$ can be analytically derived from P_2 by the probability theory [14]

$$\hat{P}_1(y_d; z_i, z_k) = \int \mathrm{d}y_k P_2(y_d + y_k, y_k; z_i, z_k)$$
$$= \frac{1}{2h\sqrt{\pi(1-\Sigma_{ik})}} \exp\left(\frac{-y_d^2}{4h^2(1-\Sigma_{ik})}\right). \quad (24)$$

Similarly, the 4D infinite integral in (19) can be reduced as

$$< A_{ik}A_{mn} >= \int \mathrm{d}y_{d1} \int \mathrm{d}y_{d2}$$
$$\hat{P}_2(y_{d1}, y_{d2}; z_i, z_k, z_m, z_n) A_{ik} A_{mn}, \quad (25)$$

where

$$\hat{P}_2(y_{d1}, y_{d2}; z_i, z_k, z_m, z_n) = \int \mathrm{d}y_k \int \mathrm{d}y_n$$
$$P_4(y_{d1} + y_k, y_k, y_{d2} + y_n, y_n; z_i, z_k, z_m, z_n). \quad (26)$$

The analytical formula of (26) can be readily derived by the Matlab symbolic toolbox and is shown in the Appendix.

V. Numerical Results

To verify the accuracy and efficiency of the modified SIE model, we use the MC-based integral equation (MIE) method proposed in [15] as the reference. The sampling length is $l = 10\eta$. The panel size of the MIE method is $\Delta z = \min(h/10, \eta/10, \delta/10)$ and that of the SIE method is $\Delta z = \eta/2$. The larger panel size used in the SIE method, typically $\eta/2$ or $\eta/4$, is intended to prevent the discretized panels from being over-correlated [16]. It should be noted that the reduction in panel number does not contribute to the computational saving as for each panel a Gaussian quadrature with at least 5 points is associated to maintain the numerical accuracy. Two Gaussian rough surfaces are tested: one is the smoother case with $h = 1\mu m, \eta = 2h$ and the other is the rougher case with $h = 1\mu m, \eta = h$. All the programming is done in Matlab and the simulations are conducted on a desktop PC with 2.8GHz CPU and 512MB memory.

To ensure that results from MIE is statistically reliable, we first perform the convergence test for the computation of $\bar{\rho}_e$. The parameters are set to be $h = \eta = \delta = 1\mu m$. As shown in Fig. 4, the mean value of ER requires more than 3000 runs to converge to within 1%, which proves the MC-based methods to be highly time-consuming. In the following analysis, we adopt the results of 1500-run MIE method as the benchmark to confirm the accuracy of the proposed SIE method.

Fig. 5 and Fig. 6 compare the ratio of $\bar{\rho}_e/\rho$ and $\bar{\mu}_e/\mu$ from the MIE method and the modified SIE method, respectively. The curves are drawn with respect to the normalized roughness h/δ. An excellent agreement is observed from $h/\delta = 0.2$ where the rough surface effects are still insignificant to $h/\delta = 2$ where the rough surface effects have been well-developed. This verifies the accuracy of the proposed SIE method. Fig. 6 proves that the internal inductance is also influenced by the surface roughness but with a different behavior.

To demonstrate the efficiency of our modified SIE formulation, we compare the CPU time among the MIE, original

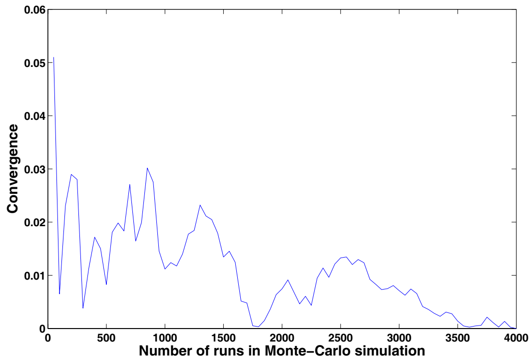

Fig. 4. Convergence test for MIE method.

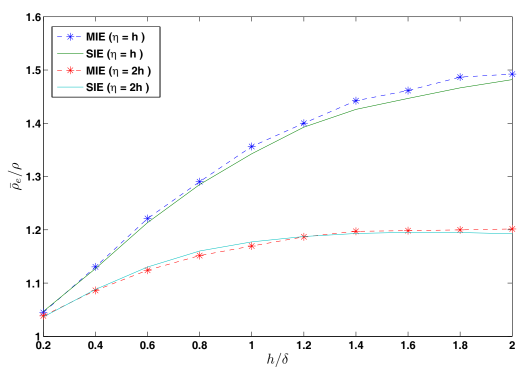

Fig. 5. Ratio of $\bar{\rho}_e/\rho$ from MIE and SIE.

SIE and modified SIE methods in the rougher case with $h = 1\mu m, \eta = h$. As shown in Table I, the modified SIE method is more than 30X faster than the original SIE method, which is due to the cut down of two folds of infinite integral in the second-order correction scheme. When compared to the MIE method, the modified SIE method provides an even higher efficiency enhancement. The computation of the SIE method can be further reduced by the matrix compression technique developed in [12], which reduces the number of explicitly-generated elements in F from $O(N^4)$ to $O(Nlog^2(N))$. Nevertheless, due to the moderate problem size in our local scope modeling, the advantages of implementing complicated matrix compression technique are easily obscured by the runtime overhead and highly involved coding in that quite a part of panels stay within the strong interaction region and thus should be calculated and stored as the standard dense matrix.

TABLE I
CPU TIME COMPARISON ($\eta = h = 1\mu m$).

h/δ	MIE(1500 runs)	SIE (Original)	SIE (Modified)
1	7160.3s	6367.3s	198.7s
2	14484.7s	6544.7s	200.3s

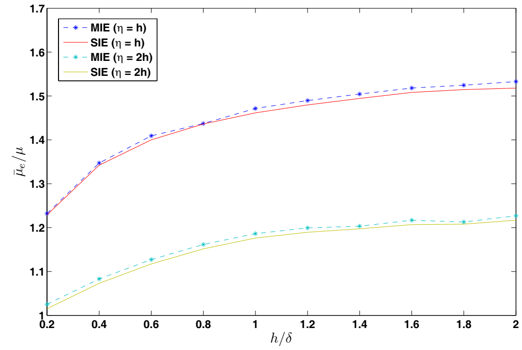

Fig. 6. Ratio of $\bar{\mu}_e/\mu$ from MIE and SIE.

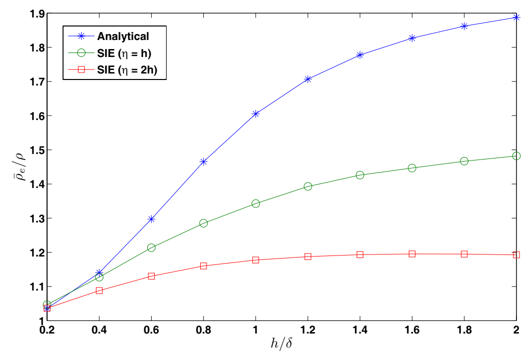

Fig. 7. Ratio of $\bar{\rho}_e/\rho$ from analytical formula and SIE.

Fig. 7 shows the comparison of the analytical formula (1) and the SIE method under the two rough surfaces that have the same RMS height. It can be seen that (1) tends to largely over-estimate the impact of surface roughness. In addition, the analytical formula cannot distinguish the two actually different cases as neglecting the information of correlation length. In contrast, the statistical formulations of ER and EP offer better resolution and flexibility through allowing various statistical models with different parameters.

VI. Conclusion

An efficient model has been proposed to enable the numerical evaluation of the random rough surface effects in internal impedance extraction for large-scale interconnect structures. The introduction of ER and EP achieves a balance between the global numerical simulation and the analytical formula by first fully modeling the influence of surface roughness within a sampling region and then extrapolating the results to the entire domain. An improved formulation for the SIE method has been presented to halve the dimension of infinite integral required in the second-order correction scheme, which substantially enhances the efficiency and preserves the deterministic nature. Numerical experiments have shown that our method can provide sufficient modeling accuracy and simulation flexibility at a mild computational cost.

VII. Acknowledgement

This material is supported in part by the Hong Kong Research Grants Council under Project HKU 7174/07E, and in part by the University Research Committee of The University of Hong Kong.

Appendix

The 2D partial probability density function $\hat{P}_2$ in (26) is derived as follows by the Symbolic toolbox of Matlab:

$$\hat{P}_2(y_{d1}, y_{d2}; z_i, z_k, z_m, z_n) = \pi\cdot\exp((-2*\Pi_{24}\cdot y_{d2}\cdot y_{d1}\cdot\Pi_{12}\cdot\Pi_{33}+2\cdot\Pi_{23}\cdot y_{d1}\cdot\Pi_{12}\cdot\Pi_{44}\cdot y_{d2}+2\cdot y_{d1}^2\cdot d11\cdot\Pi_{23}\cdot\Pi_{24}-2\cdot\Pi_{12}\cdot y_{d1}\cdot\Pi_{13}\cdot\Pi_{44}\cdot y_{d2}-\Pi_{22}\cdot y_{d1}^2\cdot d11\cdot\Pi_{44}+2\cdot\Pi_{23}\cdot y_{d1}\cdot\Pi_{11}\cdot\Pi_{34}\cdot y_{d2}+2\cdot\Pi_{23}\cdot y_{d1}\cdot\Pi_{11}\cdot\Pi_{44}\cdot y_{d2}-2\cdot\Pi_{24}\cdot y_{d2}\cdot y_{d1}\cdot\Pi_{11}\cdot\Pi_{34}-2\cdot\Pi_{24}\cdot y_{d2}\cdot y_{d1}\cdot\Pi_{11}\cdot\Pi_{33}+\Pi_{34}^2\cdot y_{d2}^2\cdot\Pi_{11}+\Pi_{12}^2\cdot y_{d1}^2\cdot\Pi_{44}+2\cdot\Pi_{14}\cdot y_{d2}^2\cdot\Pi_{24}\cdot\Pi_{33}+\Pi_{14}^2\cdot y_{d2}^2\cdot\Pi_{33}+\Pi_{44}\cdot y_{d2}^2\cdot\Pi_{13}^2+\Pi_{44}\cdot y_{d2}^2\cdot\Pi_{23}^2+\Pi_{24}^2\cdot y_{d2}^2\cdot\Pi_{33}+y_{d1}^2\cdot\Pi_{11}\cdot\Pi_{24}.^2+y_{d1}^2\cdot\Pi_{11}\cdot\Pi_{23}^2+\Pi_{12}^2\cdot y_{d1}^2\cdot\Pi_{33}-2\cdot\Pi_{22}\cdot y_{d1}^2\cdot\Pi_{11}\cdot\Pi_{34}+\Pi_{22}\cdot y_{d1}^2\cdot\Pi_{13}^2+\Pi_{22}\cdot y_{d1}^2\cdot\Pi_{14}^2+\Pi_{22}\cdot\Pi_{34}^2\cdot y_{d2}^2-2\cdot\Pi_{13}\cdot\Pi_{14}\cdot y_{d2}^2\cdot\Pi_{34}-\Pi_{22}\cdot y_{d1}^2\cdot\Pi_{11}\cdot\Pi_{33}-2\cdot y_{d1}\cdot\Pi_{14}\cdot y_{d2}\cdot\Pi_{13}\cdot\Pi_{23}-2\cdot\Pi_{14}\cdot y_{d2}^2\cdot\Pi_{23}\cdot\Pi_{34}-\Pi_{44}\cdot y_{d2}^2\cdot\Pi_{33}\cdot\Pi_{11}-2\cdot\Pi_{23}\cdot y_{d1}^2\cdot\Pi_{12}\cdot\Pi_{13}-2\cdot\Pi_{23}\cdot y_{d1}^2\cdot\Pi_{12}\cdot\Pi_{14}+2\cdot\Pi_{14}\cdot y_{d2}\cdot y_{d1}\cdot\Pi_{33}\cdot\Pi_{12}-2\cdot\Pi_{22}\cdot\Pi_{34}\cdot y_{d2}\cdot\Pi_{13}\cdot y_{d1}+2\cdot\Pi_{22}\cdot\Pi_{14}\cdot y_{d2}\cdot y_{d1}\cdot\Pi_{33}-\Pi_{22}\cdot\Pi_{44}\cdot y_{d2}^2\cdot\Pi_{33}+2\cdot\Pi_{22}\cdot y_{d1}^2\cdot\Pi_{13}\cdot\Pi_{14}+2\cdot\Pi_{23}\cdot y_{d1}\cdot\Pi_{34}\cdot y_{d2}\cdot\Pi_{12}+2\cdot\Pi_{22}\cdot y_{d1}\cdot\Pi_{14}\cdot y_{d2}\cdot\Pi_{34}-2\cdot\Pi_{22}\cdot\Pi_{44}\cdot y_{d2}\cdot\Pi_{13}\cdot y_{d1}-2\cdot\Pi_{44}\cdot y_{d2}^2\cdot\Pi_{33}\cdot\Pi_{12}+2\cdot\Pi_{44}\cdot y_{d2}^2\cdot\Pi_{13}\cdot\Pi_{23}-2\cdot\Pi_{24}\cdot y_{d2}\cdot y_{d1}\cdot\Pi_{12}\cdot\Pi_{34}+2\cdot\Pi_{12}^2\cdot y_{d1}^2\cdot\Pi_{34}-2\cdot\Pi_{34}\cdot y_{d2}^2\cdot\Pi_{23}\cdot\Pi_{24}-2\cdot\Pi_{24}\cdot y_{d1}^2\cdot\Pi_{12}\cdot\Pi_{14}+2\cdot\Pi_{34}^2\cdot y_{d2}^2\cdot\Pi_{12}-2\cdot\Pi_{24}\cdot y_{d1}^2\cdot\Pi_{12}\cdot\Pi_{13}+2\cdot\Pi_{12}\cdot y_{d1}\cdot\Pi_{14}\cdot y_{d2}\cdot\Pi_{34}+2\cdot\Pi_{24}^2\cdot y_{d2}\cdot y_{d1}\cdot\Pi_{13}+2\cdot\Pi_{24}\cdot y_{d2}\cdot y_{d1}\cdot\Pi_{13}^2-2\cdot\Pi_{24}\cdot y_{d2}\cdot y_{d1}\cdot\Pi_{14}\cdot\Pi_{23}+2\cdot\Pi_{24}\cdot y_{d2}\cdot y_{d1}\cdot\Pi_{13}\cdot\Pi_{23}+2\cdot\Pi_{24}\cdot y_{d2}\cdot y_{d1}\cdot\Pi_{13}\cdot\Pi_{14}-2\cdot y_{d1}\cdot\Pi_{14}^2\cdot y_{d2}\cdot\Pi_{23}-2\cdot y_{d1}\cdot\Pi_{14}\cdot y_{d2}\cdot\Pi_{23}^2-2\cdot\Pi_{34}\cdot y_{d2}\cdot\Pi_{12}\cdot y_{d1}\cdot\Pi_{13}-2\cdot\Pi_{34}\cdot y_{d2}^2\cdot\Pi_{13}\cdot\Pi_{24})/a/(\Pi_{44}\cdot\Pi_{22}-2\cdot\Pi_{23}\cdot\Pi_{24}-2\cdot\Pi_{14}\cdot\Pi_{24}-2\cdot\Pi_{14}\cdot\Pi_{23}-\Pi_{24}^2-\Pi_{23}^2-\Pi_{14}^2-\Pi_{13}^2-2\cdot\Pi_{13}\cdot\Pi_{24}+\Pi_{44}\cdot\Pi_{11}+2\cdot\Pi_{44}\cdot\Pi_{12}+2\cdot\Pi_{34}\cdot\Pi_{22}+2\cdot\Pi_{34}\cdot\Pi_{11}+\Pi_{33}\cdot\Pi_{22}+\Pi_{33}\cdot\Pi_{11}+2\cdot\Pi_{33}\cdot\Pi_{12}-2\cdot\Pi_{13}\cdot\Pi_{23}+4\cdot\Pi_{34}\cdot\Pi_{12}-2\cdot\Pi_{13}\cdot\Pi_{14}))/b/((2\cdot\Pi_{12}+\Pi_{11}+\Pi_{22})/a)^{1/2}/((\Pi_{44}\cdot\Pi_{22}-2\cdot\Pi_{23}\cdot\Pi_{24}-2\cdot\Pi_{14}\cdot\Pi_{24}-2\cdot\Pi_{14}\cdot\Pi_{23}-\Pi_{24}^2-\Pi_{23}^2-\Pi_{14}^2-\Pi_{13}^2-2\cdot\Pi_{13}\cdot\Pi_{24}+\Pi_{44}\cdot\Pi_{11}+2\cdot\Pi_{44}\cdot\Pi_{12}+2\cdot\Pi_{34}\cdot\Pi_{22}+2\cdot\Pi_{34}\cdot\Pi_{11}+\Pi_{33}\cdot\Pi_{22}+\Pi_{33}\cdot\Pi_{11}+2\cdot\Pi_{33}\cdot\Pi_{12}-2\cdot\Pi_{13}\cdot\Pi_{23}+4\cdot\Pi_{34}\cdot\Pi_{12}-2\cdot\Pi_{13}\cdot\Pi_{14})/a/(2\cdot\Pi_{12}+\Pi_{11}+\Pi_{22}))^{(1/2)}$$

where Π is the inverse of the correlation matrix Σ defined in (20). $a = 2\sigma^2$ and $b = 4\pi^2\sigma^4\sqrt{|\Pi|}$.

References

[1] M. Nakhla and R. Achar, *Fundamentals of Multiconductor Transmission Line Analysis*. Canada: Omniz Global Knowledge, 2002.

[2] H. Tanaka, "Precise measurements of dissipation factor in microwave printed circuit boards," *IEEE Trans. Instrum. Meas.*, vol. 38, no. 2, pp. 509–514, 1989.

[3] T. Nakagawa, "The relationship between self-annealing of plated copper and copper surface treatment," *J. Circuit World*, vol. 29, no. 3, pp. 22–26, 2003.

[4] E. Hammerstad and O. Jensen, "Accurate models for microstrip computer-aided design," in *IEEE Microwave Symposium Digest, MTT-S International*, 1980, pp. 407–409.

[5] L. Proekt and A. C. Cangellaris, "Investigation of the impact of conductor surface roughness on interconnect frequency-dependent ohmic loss," in *Proc. Intl. Conf. on Electronic Components and Technology*, 2003, pp. 1004–1010.

[6] Q. Chen and N. Wong, "A stochastic integral equation method for resistance extraction of conductors with random rough surfaces," in *Proc. IEEE Intl. Symp. on Intelligent Signal Processing and Communication Systems*, 2006, pp. 411–414.

[7] S. P. Morgan, "Effect of surface roughness on eddy current losses at microwave frequencies," *J. Applied Physics*, vol. 20, no. 3, pp. 352–362, 1949.

[8] M. Kamon, M. J. Tsuk, and J. K. White, "Fasthenry: a multipole-accelerated 3-d inductance extraction program," *IEEE Trans. Microw. Theory Tech.*, vol. 42, no. 9, pp. 1750–1758, 1994.

[9] L. Tsang, J. A. Kong, K. H. Ding, and C. O. Ao, *Scattering of electromagnetic waves, Vol. 2, Numerical simulations*. New York: Wiley, 2001.

[10] Z. Zhu, "Efficient integral equation based algorithms for parasitic extraction of interconnects with smooth or rough surface," Ph.D. dissertation, Department of Electrical Engineering and Computer Science, Massachusetts Institute of Technology, Aug. 2004.

[11] Z. Zhu, A. Demir, and J. White, "A stochastic integral equation method for modeling the rough surface effect on interconnect capacitance," in *Proc. IEEE Intl. Conf. on Computer Aided-Design*, 2004, pp. 887–891.

[12] Z. Zhu and J. White, "Fastsies: a fast stochastic integral equation solver for modeling the rough surface effect," in *Proc. IEEE Intl. Conf. on Computer Aided-Design*, 2005, pp. 675–682.

[13] P. J. Davis and P. Rabinowitz, *Methods of numerical integration*. Orlando: Acedemic press Inc., 1984.

[14] A. Papoulis, *Probability, Random Variables, and Stochastic Processes*. New York: McGraw-Hill, 2001.

[15] L. Tsang, X. Gu, and H. Braunisch, "Effects of random rough surface on absorption by conductors at microwave frequencies," *IEEE Microw. Wireless Compon. Lett.*, vol. 16, no. 4, pp. 221–223, 2006.

[16] M. Kleiber and T. D. Hien, *The stochastic finite element method*. England: Wiley, 1992.